

# Tests on NaI(Tl) crystals for WIMP search at the Yangyang Underground Laboratory

K.W. Kim<sup>b</sup>, W.G. Kang<sup>a</sup>, S.Y. Oh<sup>e</sup>, P. Adhikari<sup>e</sup>, J.H. So<sup>a</sup>, N.Y. Kim<sup>a</sup>, H.S. Lee<sup>c,\*</sup>, S. Choi<sup>b</sup>, I.S. Hahn<sup>d</sup>,  
E.J. Jeon<sup>a</sup>, H.W. Joo<sup>b</sup>, B.H. Kim<sup>b</sup>, H.J. Kim<sup>f</sup>, Y.D. Kim<sup>a,e,\*</sup>, Y.H. Kim<sup>a,g</sup>, J.K. Lee<sup>b</sup>, D.S. Leonard<sup>h</sup>,  
J. Li<sup>a</sup>, S.L. Olsen<sup>b</sup>, H.S. Park<sup>g</sup>

<sup>a</sup>Center for Underground Physics, Institute for Basic Science (IBS), Daejeon 305-811, Korea

<sup>b</sup>Department of Physics and Astronomy, Seoul National University, Seoul 151-747, Korea

<sup>c</sup>Department of Physics, Ewha Womans University, Seoul 120-750, Korea

<sup>d</sup>Department of Science Education, Ewha Womans University, Seoul 120-750, Korea

<sup>e</sup>Department of Physics, Sejong University, Seoul 143-747, Korea

<sup>f</sup>Department of Physics, Kyungpook National University, Daegu 702-701, Korea

<sup>g</sup>Korea Research Institute of Standards and Science, Daejeon 205-340, Korea

<sup>h</sup>Department of Physics, University of Seoul, Seoul 130-743, Korea

---

## Abstract

Among the direct searches for WIMP-type dark matter, the DAMA experiment is unique in that it has consistently reported a positive signal for an annual-modulation signal with a large ( $9.3\sigma$ ) statistical significance. This result is controversial because if it is interpreted as a signature for WIMP interactions, it conflicts with other direct search experiments that report null signals in the regions of parameter space that are allowed by the DAMA observation. This necessitates an independent verification of the origin of the observed modulation signal using the same technique as that employed by the DAMA experiment, namely low-background NaI(Tl) crystal detectors. Here, we report first results of a program of NaI(Tl) crystal measurements at the Yangyang Underground Laboratory aimed at producing NaI(Tl) crystal detectors with lower background levels and higher light yields than those used for the DAMA measurements.

**Keywords:** Dark Matter, WIMP, KIMS, NaI(Tl) crystal

**PACS:** 29.40.Mc, 85.60.Ha

---

## 1. Introduction

Numerous astronomical observations have led to the conclusion that most of the matter in the Universe is invisible, exotic, and nonrelativistic dark matter [1, 2]. However, in spite of a considerable amount of experimental effort, the nature of the dark matter remains unknown. Weakly interacting massive particles (WIMPs) are one of the most attractive candidates for dark matter particles [3, 4]. In supersymmetric models for beyond the standard model physics, the lightest supersymmetric particle (LSP) is a natural candidate for WIMP-type dark

matter. A number of experiments have made direct searches for a WIMP component of our Galaxy by looking for evidence for WIMP-nucleus scattering by detecting the recoiling nucleus in ultra-sensitive low-background detectors [5, 6].

The DAMA experiment searches for an annual modulation in the detection rate of nuclear recoils in an array of ultra-low-background NaI(Tl) crystals caused by the Earth's orbital motion through our Galaxy's dark-matter halo [7, 8, 9]. This experiment, which has been operating for over 15 years, has consistently reported a positive signal for an annual modulation with a phase that is consistent with expectations for motion of the Earth relative to the Galactic rest frame. The statistical significance of the DAMA annual modulation signal has now reached  $9.3\sigma$ . Other experiments, including CoGeNT [10, 11, 12], CRESST [13], and

---

\*Corresponding authors, Tel:+82-2-3277-3413; fax:+82-2-3277-2372

Email addresses: hyunsulee@ewha.ac.kr (H.S. Lee),  
ydkim@ibs.re.kr (Y.D. Kim)

CDMS [14], have also reported signals that could be interpreted as being possibly due to WIMP interactions. However, these signals have marginal significance at the  $<3\sigma$  confidence level and some inconsistencies with null results using similar detectors that were already reported [15, 16, 17]. Nevertheless, these marginal signals have motivated the same experimental groups and, in some cases, independent groups to devise experiments to check these signals using similar techniques but with higher sensitivity. In contrast, to date, no independent verification of the DAMA signal in an experiment using the same technique has been done.

The DAMA signal, in particular its interpretation as being due to WIMP-nucleus scattering, has been the subject of a continuing debate that started with the first DAMA report 15 years ago. This is because the WIMP-nucleon cross sections inferred from the DAMA modulation are in conflict with limits from other experiments that directly measure the total rate of nuclear recoils, such as XENON100 [18], LUX [19], and SuperCDMS [20]. However, room remains for explaining all of these experimental results without conflict in terms of nontrivial systematic differences in detector responses [21, 22] and the commonly used astronomical model for the WIMP distribution [23]. An unambiguous verification of the DAMA signal by an independent experiment using similar NaI(Tl) crystals is mandatory.

Reproducing the DAMA measurement requires the independent development of ultra-low-background NaI(Tl) crystals. This is because the crystal-growing company<sup>1</sup> that supplied the DAMA NaI(Tl) crystals will not produce the same crystals for other experimental groups. Recently, the ANAIS group has been developing ultra-low-background NaI(Tl) crystals with the goal of reproducing the DAMA result [24, 25] and the DM-Ice group reports background measurements of NaI(Tl) crystals [26]. However, to date, no experimental group has produced NaI(Tl) crystals with background levels at or below than those used in the DAMA experiment.

The Korea Invisible Mass Search (KIMS) Collaboration has been performing direct WIMP searches using ultra-low-background CsI(Tl) crystal detectors, which are similar experimental devices to the NaI(Tl) crystals used in the DAMA experiment.

This implementation required extensive research and development aimed at identifying and reducing internal backgrounds in the CsI crystals [27, 28]. Null results from KIMS reject WIMP-Iodine nuclei interactions as the source of the DAMA signal with very little model dependence [29, 30]. However, because the DAMA results can be interpreted as being primarily due to WIMP-sodium nuclei interactions, which, for example, would be the case for low-mass WIMPs, it remains necessary to confirm the DAMA observations with NaI(Tl) crystal detectors. This motivated a program to develop ultra-low-background NaI(Tl) crystal detectors with lower background levels and higher light yields (and, thus, a lower energy threshold) than those of the DAMA experiment in order to identify unambiguously the origin of the DAMA modulation signature.

## 2. Experimental Setup

To evaluate the NaI(Tl) crystals, we use the experimental setup that was used for the KIMS CsI(Tl) detector measurements at the Yangyang Underground Laboratory (Y2L), which has a 700 m earth overburden (2400 m water equivalent). This includes a 12-module array of CsI(Tl) detectors (total mass of 103.4 kg) inside a shield that consists, from inside out, of 10 cm of copper, 5 cm of polyethylene, 15 cm of lead, and 30 cm of liquid-scintillator-loaded mineral oil to stop external neutrons, gamma rays, and veto cosmic ray muons. Each detection module consists of a low-background CsI(Tl) crystal ( $8 \times 8 \times 30 \text{ cm}^3$ ) with a photomultiplier tube (PMT) mounted at each end.

Two NaI(Tl) crystals were mounted inside the CsI(Tl) detector array as shown in Fig. 1. In November 2013, we installed the first NaI(Tl) crystal, NaI-001, in the CsI array; the second NaI(Tl) crystal, NaI-002, was added in February 2014, soon after that crystal was delivered and assembled.

### 2.1. NaI(Tl) crystals

The two NaI(Tl) crystals were produced by the Alpha Spectra Company.<sup>2</sup> The crystals were grown from NaI powder that was not of the highest attainable purity; the initial purification was carried out by Alpha Spectra. The crystals have a cylindrical shape and were cut from a 32 inch ingot that was

<sup>1</sup>Crismatec, France

<sup>2</sup><http://www.alphaspectra.com>

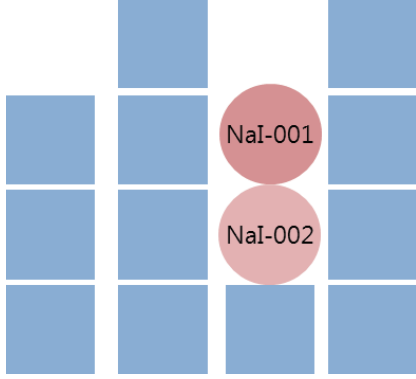


Figure 1: Schematic test setup for two NaI(Tl) crystals (circles) with 12 CsI(Tl) crystals (squares).

grown by the Kyropoulos method. The detailed sizes of the crystals are listed in Table 1. After the crystal surfaces were polished they were wrapped with a Teflon reflector and inserted into an oxygen-free electronic (OFE) copper cylinder and encapsulated in a nitrogen gas environment. There is a 12.7-mm-thick quartz-plate window at each end of the cylinder, with optical grease between the crystal and the quartz windows. A 3" PMT is mounted at each end of the cylinder.

### 2.2. Electronics

Each NaI crystal PMT signal was split and amplified by factors of 30 and 2; the amplified signals were digitized by 400- and 64-MHz flash analog-to-digital converters (FADC), respectively. The corresponding amplification factors for the CsI crystal PMTs were  $\times 100$  and  $\times 10$ . The total recorded time window for an event was 40  $\mu$ s, of which 5  $\mu$ s is analyzed for the NaI(Tl) crystals and 25  $\mu$ s is analyzed for the CsI(Tl) crystals, reflecting the different decay times of the two materials.

Figure 2 shows a schematic diagram of the detector setup. The trigger condition for the CsI(Tl) crystals is two or more photoelectrons (PEs) in each PMT within a 2- $\mu$ s time window. The NaI(Tl) crystals have a reduced PE requirement of one PE in each PMTs within a 200 ns window in order to have a minimal trigger bias and a low energy threshold.

The muon rate at Y2L is  $(7.0 \pm 0.4) \times 10^{-8}/\text{s}/\text{cm}^2/\text{sr}$  [31]. Since the KIMS muon veto system was under maintenance, no muon veto is applied to the data reported here. Approximately 3~4 muons pass through each crystal per day. These induce low-energy events with observed energies  $< 10$

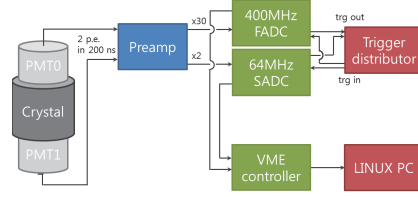


Figure 2: Schematic electronics diagram of the KIMS NaI experiment.

keV during a few second time interval after a muon passes through the crystal because of a long decay-time component of the NaI(Tl) scintillation process. However, most of these events are rejected by the selection requirements discussed in Section 6 and, so, cosmic ray muon-related events are negligible in the data reported here.

## 3. Signal Calibrations

The energy calibration of the NaI(Tl) crystals was done with a  $^{241}\text{Am}$  source. The detector had one hole of 10 mm in diameter covered by 127- $\mu$ m-thick aluminum foil in the center of the encapsulating Cu container. The source was located in front of the hole. The CsI(Tl) crystal calibration procedure is described in Refs. [29, 30].

### 3.1. Photomultiplier tubes

Two different types of low-background PMTs were tested: a metal-packed R11065 and a glass-packed R12669, both manufactured by Hamamatsu Photonics.<sup>3</sup> Table 2 shows the specifications for each PMT. The R12669 PMT is a modified version of the R6233 Super Bialkali (SBA) PMT used by DAMA in its recent upgrade [32]. The PMTs we used were selected for their high quantum efficiency. The radioactivity levels of the PMTs were measured at underground with a HPGe detector. As expected, the metal PMT has a lower radioactivity level than the glass PMT as listed in Table 2. However, the 3" R12669 PMTs suffer from serious nonlinearity when the signal height is  $> 1$  V (corresponding to about 1 MeV in energy), and therefore, the high-energy region of the NaI(Tl) crystal data taken with these PMTs was not analyzed in this study.

<sup>3</sup><http://www.hamamatsu.com/>

Table 1: Specifications of the NaI(Tl) crystals used in this study. The last two columns are the dates the crystals were grown and transported to Y2L. “Transp” indicates the means by which the crystals were transported from the United State to Korea.

Crystal	Size	Mass	Transp	T (Growth)	T (underground)
NaI-001	5''(D) $\times$ 7''(L)	8.26	Air	2011.9	2013.9
NaI-002	4.2''(D) $\times$ 11''(L)	9.2	Sea	2013.4	2014.1

Table 2: Specifications for PMTs tested in this study. Radioactivity levels measured with a HPGe detector at Y2L. SEL means “selected for high quantum efficiency.”

PMT		R12669SEL <sup>b</sup>	R11065SEL <sup>b</sup>
Photocathode		SBA	Bialkali
Window		Borosilicate	Quartz
Body		Borosilicate	Kovar
Stem		Glass	Glass
Gain (HV)		$1 \times 10^6$	$5 \times 10^6$
Radioactivity <sup>a</sup> (mBq/PMT)	U( <sup>214</sup> Bi)	$25 \pm 5$	$60 \pm 5$
	Th( <sup>228</sup> Ac)	$12 \pm 5$	$0.5 \pm 0.2$
	K( <sup>40</sup> K)	$58 \pm 5$	$19 \pm 2$
	<sup>226</sup> Ra	$60 \pm 10$	$5 \pm 2$
	<sup>208</sup> Tl	$4 \pm 1$	—

### 3.2. Single-photoelectron spectra

For low-energy events, the 400-MHz FADC waveforms were analyzed to identify clusters of single PEs (SPEs) [33]. The charge distribution of a SPE, obtained by identifying isolated clusters at the decay tail of the signal (2–5  $\mu$ s after the signal start) in order to suppress multiple PE clusters, is shown in Fig. 3.

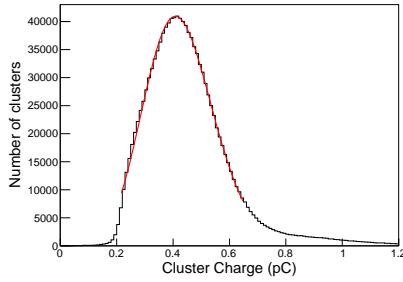


Figure 3: The SPE charge distribution measured with the NaI-001 crystal readout by an R12669 PMT. This distribution is produced with a <sup>241</sup>Am calibration source in a time window that is 2–5  $\mu$ s after the signal start to reduce PE pileup.

### 3.3. Light yields

Figure 4 shows the distribution of the number of PEs obtained using an <sup>241</sup>Am source with the NaI-001 and NaI-002 detectors read out with different types of PMTs. The mean number of PEs detected with the R12669 PMTs is 22% greater than that detected by the R11065 PMTs. This is consistent with the ANAIS test [24] and reflects the higher quantum efficiency of the SBA photocathode.

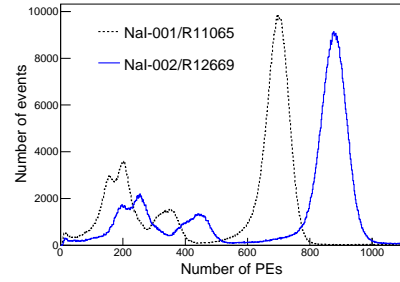


Figure 4: The measured number of PEs with the <sup>241</sup>Am source calibration for the NaI-001 and NaI-002 crystals read out by two different PMT types.

### 3.4. Scintillation decay time

We study the scintillation decay time of the NaI(Tl) crystals from the time response to signals



Table 3: Backgrounds from the internal radioactive contaminants in the NaI(Tl) crystals. The units for all the values are mBq/kg. For “Total alphas,” each alpha particle is counted as one decay.

Radionuclei	NaI-001	NaI-002
$^{238}\text{U}$ (by $^{214}\text{Bi}$ )	$<0.0003$	$<0.0015$
$^{228}\text{Th}$ (by $^{216}\text{Po}$ )	$<0.013$	$0.002 \pm 0.001$
$^{40}\text{K}$	$1.25 \pm 0.09$	$1.49 \pm 0.07$
$^{210}\text{Pb}$	$3.28 \pm 0.01$	$1.76 \pm 0.01$
Total alphas	$3.29 \pm 0.01$	$1.77 \pm 0.01$

induced by a radioactive  $\gamma$ -ray source. Figure 5 shows the integrated signal shapes for 59.54 keV  $\gamma$ -rays from a  $^{241}\text{Am}$  source. The data are fitted with two exponentials with time constants of 0.22 and  $1.17 \mu\text{s}$ . The fast component accounts for  $\sim 83\%$  of the total light yield.

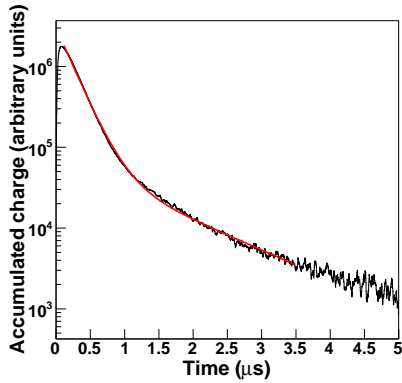


Figure 5: Scintillation decay time spectrum of the NaI-001 crystal obtained with  $^{241}\text{Am}$  source data and fitted with two exponential functions.

#### 4. Natural background

To produce ultra-low-background crystals, contamination from internal natural radioisotopes has to be reduced. Table 3 shows the measured results of the internal backgrounds for the two crystals. In this section we describe some details of these measurements.

##### 4.1. $^{40}\text{K}$ background

The most serious internal background contamination is  $^{40}\text{K}$  because of the low-energy x-ray that

is produced during its electron capture decay process, which proceeds via a transition to an excited state of  $^{40}\text{Ar}$  with a branching ratio of 10%. This decay generates a  $\sim 3$  keV x-ray in coincidence with a 1460 keV  $\gamma$ -ray. If the accompanying 1460 keV  $\gamma$ -ray escapes from the crystal, the event consists of a single 3 keV hit. The  $^{40}\text{K}$  level in the DAMA crystals is in the 10–20 ppb range [34].

We studied coincidence signals between NaI ( $\sim 3$  keV) and CsI (1460 keV) detectors to identify unambiguous  $^{40}\text{K}$  decays. Figure 6(a) shows a scatterplot of NaI *versus* CsI detector reponse without the application of any of the requirements used to remove PMT noise-induced signals that are discussed in Section 6 below; Fig. 6(b) shows the same plot after the application of these requirements. In Fig. 6(b), the event cluster near 3 keV in NaI and 1460 keV in a surrounding CsI crystal is from  $^{40}\text{K}$  decays. Another, smaller cluster near  $\sim 1$  keV in the NaI and 1270 keV in one of the CsI crystals is from  $^{22}\text{Na}$  decays. By comparing the rate for  $^{40}\text{K}$  induced events with a Geant4-based detector simulation [35] for the CsI and NaI crystal setup, we determine the  $^{40}\text{K}$  contamination in the NaI crystals to be  $41.4 \pm 3.0$  ppb ( $1.25 \pm 0.09$  mBq/kg) and  $49.3 \pm 2.4$  ppb ( $1.49 \pm 0.07$  mBq/kg), respectively, for NaI-001 and NaI-002. This is close to the  $^{40}\text{K}$  levels measured in the ANAIS-25 crystals [24, 36].

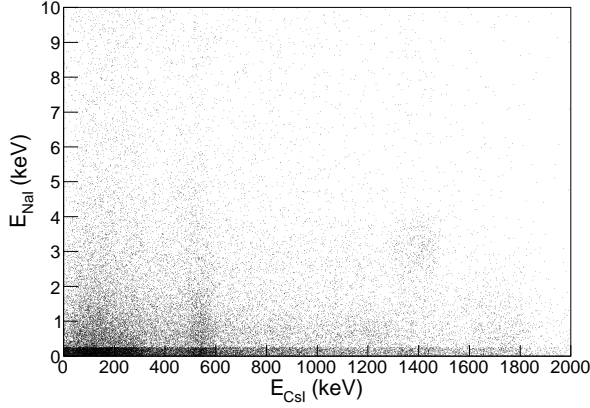
##### 4.2. $^{238}\text{U}$ background

Although the PMTs are nonlinear at high light output, alpha-induced events inside the crystal can be identified by the mean time of the signal, defined as

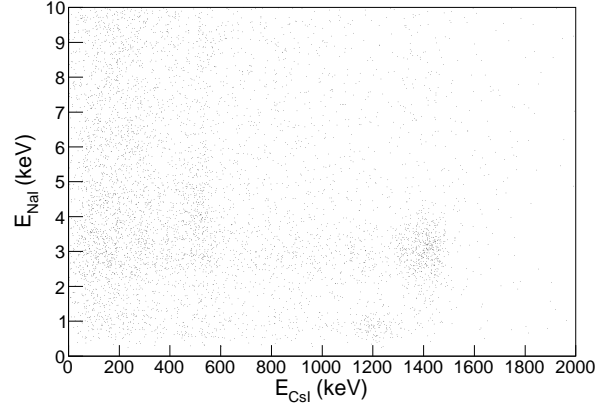
$$\langle t \rangle \equiv \frac{\sum_i A_i t_i}{\sum_i A_i}. \quad (1)$$

Here  $A_i$  and  $t_i$  are the charge and time of each cluster (for low energies) or digitized bin (for high energies). Figure 7 shows a scatter plot of the pulse height *versus* mean time for event signals from NaI-001. Alpha-induced events are clearly separated from gamma-induced events in the high-energy region because of the faster decay times of alpha-induced signals.

Because of the nonlinearity of high-energy signals, alpha particles from different nuclides cannot be distinguished event-by-event by their measured energies. Instead we determine the level of  $^{238}\text{U}$  chain contaminants by exploiting the  $^{214}\text{Po}$  237  $\mu\text{s}$  mean lifetime that occurs between  $^{214}\text{Bi}$   $\beta$ -decay and  $^{214}\text{Po}$   $\alpha$ -decay, a technique that was used



(a) No cut



(b) After PMT noise cuts

Figure 6: Scatter plots of energy in a NaI(Tl) crystal ( $E_{\text{NaI}}$ ) versus that in a surrounding CsI(Tl) crystal ( $E_{\text{CsI}}$ ) before (a) and after (b) the application of event selection requirements that remove PMT noise events. The cluster at 3 keV is due to  $^{40}\text{K}$  and that at 1 keV is due to  $^{22}\text{Na}$ .

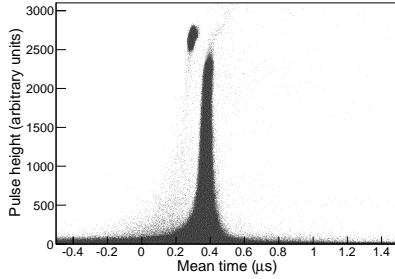


Figure 7: A scatter plot of maximum height versus mean time of event signals from NaI-001. Alpha-induced events are well separated from  $\gamma$ -induced signals because of their shorter decay time.

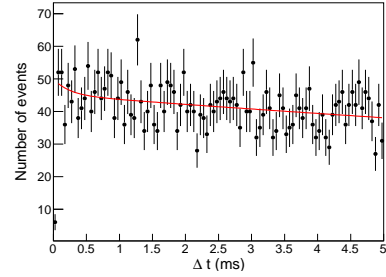


Figure 8: The  $\beta$ - $\alpha$  coincidence time spectrum from the NaI-001 crystal. There is no significant exponential decay from a  $^{214}\text{Bi}$   $\beta$  and  $^{214}\text{Po}$   $\alpha$ -decay component and an upper limit is determined from the fit.

successfully for contamination measurements in the KIMS CsI crystals [28]. Figure 8 shows the distribution of measured time intervals between an alpha-induced event and its immediately preceding event. Since there is no significant exponential component observed with the  $237\text{-}\mu\text{s}$  decay time of  $^{214}\text{Po}$ , an upper limit on the activity level is determined. This analysis shows that the contamination levels from the  $^{238}\text{U}$  chain are already sufficiently low for a WIMP dark matter search.

#### 4.3. $^{232}\text{Th}$ background

Contamination from the  $^{232}\text{Th}$  chain is studied by using  $\alpha$ - $\alpha$  time interval measurements in the crystals. In this case we look for a  $^{216}\text{Po}$   $\alpha$ -decay

component with a mean time of 209 ms following its production via  $^{220}\text{Rn} \rightarrow ^{216}\text{Po}$   $\alpha$ -decay. Figure 9 shows the distribution of the time difference between two alpha events. As one can see in Fig. 9, there is a small exponential component with the  $^{216}\text{Po}$  decay time in NaI-001; there is no such signal in NaI-002 and we set an upper limit for the contamination in that crystal. These  $\alpha$ - $\alpha$  event rates can translate into contamination levels from the  $^{228}\text{Th}$  series in the  $^{232}\text{Th}$  chain. The  $^{232}\text{Th}$  contamination levels of the two crystals, listed in Table 3, are also sufficiently low.

#### 4.4. $^{210}\text{Pb}$ background

The levels of  $^{238}\text{U}$  and  $^{232}\text{Th}$  contamination measured in both crystals are too low to account for

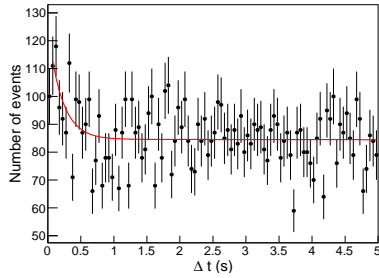


Figure 9: The time difference distribution between two alpha events in the NaI-001 crystal. The exponential component below 1 s is due to the sequential decays of  $^{220}\text{Rn}$  and  $^{216}\text{Po}$ .

the total observed alpha particle rate, which suggests that they are due to decays of  $^{210}\text{Po}$  nuclei that originate from  $^{222}\text{Rn}$  contamination that occurred sometime during the powder and/or crystal processing stages. This is confirmed by the observation of a 46-keV  $\gamma$  peak that is characteristic of  $^{210}\text{Pb}$ .

The time change in the total alpha rate provides information about when the  $^{222}\text{Rn}$  contamination occurred. After  $^{222}\text{Rn}$  contamination, the number of  $^{210}\text{Pb}$  nuclei increases as does the  $^{210}\text{Po}$   $\alpha$ -decay rate. After about three years, equilibrium is reached and the  $^{210}\text{Po}$  activity becomes constant. Figure 10 shows the total alpha rates in the two crystals as a function of data-taking time (days). The NaI-001 and NaI-002 crystals emit about 2344 and 1334 alpha particles per day, respectively. After considering the crystal masses, we find that the NaI-002 alpha activity is less than that for NaI-001 by almost a factor of two. Moreover, we also see that the NaI-002 crystal's alpha activity is increasing with time.

For  $^{210}\text{Po}$ , the alpha activity will increase as

$$R_\alpha(t) \approx A(1 - e^{-(t-t_0)/\tau_{\text{Po}}}), \quad (2)$$

where  $\tau_{\text{Po}}$  is the decay time of  $^{210}\text{Po}$  (200 days) and  $t_0$  is the time the initial  $^{210}\text{Pb}$  contamination occurred, assuming that the contamination happened suddenly. The measured alpha rate was fitted to this equation, and the results indicate that the contamination occurred at the end of April, 2013. This coincides with the time that the crystal was grown, and we conclude that the contamination occurred then.

## 5. Background from cosmic excitation

The two crystals were transported from the U.S. to Korea by different means, NaI-001 by air and NaI-002 by sea, in order to understand the cosmogenic-activation-dependence on the delivery method. Figure 11(a) shows the energy spectra for the NaI-001 crystal during the first week and for a week-long period after a 64-day delay after the arrival of the crystal underground. Figure 11(b) shows the difference between the first and second measurements. The peak at 68.7-keV is the sum of  $\gamma$ -rays and x-rays from  $^{125}\text{I}$  electron capture decay. The lower energy peak also can be identified as originating from iodine and tellurium decays. We found significantly lower cosmogenic activation in the NaI-002 crystal, and we conclude that surface transportation is mandatory for low-background crystals.

$^{22}\text{Na}$  can be produced through the  $(n, 2n)$  reaction on  $^{23}\text{Na}$  by energetic cosmic neutrons at sea level. It decays via positron emission (90%) and electron capture (10%) followed by 1270-keV gamma emission with a mean lifetime of 3.8 years. The electron capture decay produces  $\sim 0.8$  keV x-rays. Therefore about 10% of the  $^{22}\text{Na}$  decay will produce 0.8-keV x-rays and 1270-keV  $\gamma$ -rays at the same time. The  $\gamma$ - $\gamma$  coincidences show up in Fig. 6 as a cluster of events below the  $^{40}\text{K}$  decay events. The more frequent  $\beta^+$  decay channel does not generate low-energy x-rays. The 0.8-keV events are useful for studying selection efficiencies in the 1-keV energy region.

## 6. PMT noise background

Photomultiplier tubes are known to generate low-energy noise signals primarily via four different mechanisms. First, radioactive decays of U, Th, and K inside the PMT materials generate ultra-violet and/or visible photons directly inside the PMTs. Second, the high voltage applied to the PMT can cause charge to accumulate somewhere in the PMT and subsequently discharge, producing a flash. Third, PMT dark currents will produce accidental coincidences between two PMTs that satisfy the trigger condition. Fourth, large pulses can result from afterpulsing produced by ionized residual gas inside the PMT. In fact, PMT noise involves complex phenomena that are far from being completely understood.

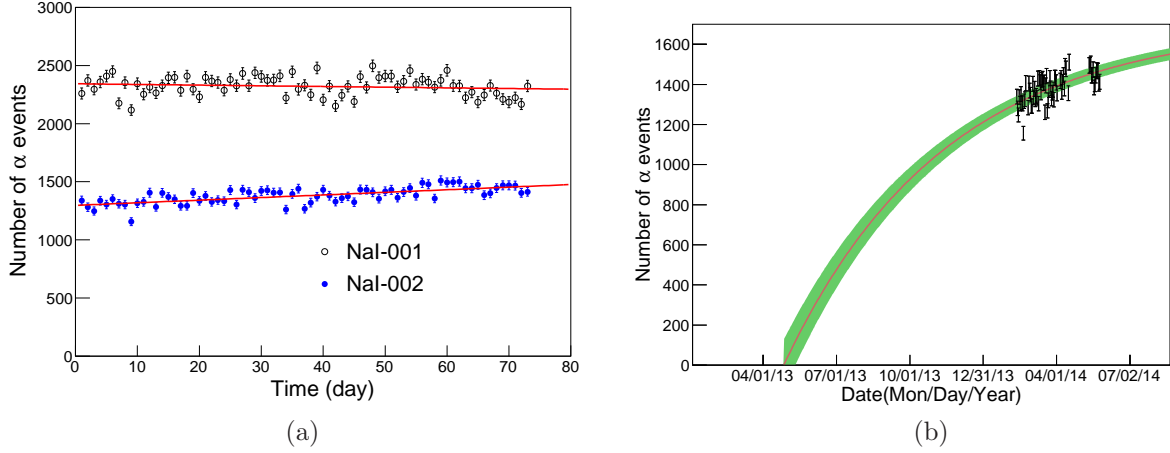


Figure 10: (a) Total number of alpha particles per day for the two NaI detectors. (b) The alpha activity increase in NaI-002 is fitted with a model in which a nearly instantaneous  $^{210}\text{Pb}$  contamination is assumed.

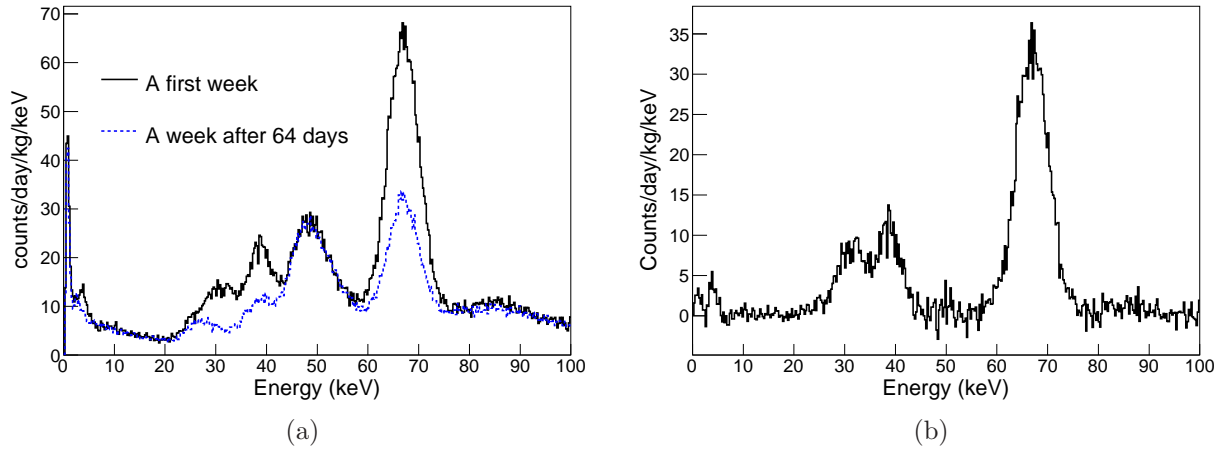


Figure 11: (a) Energy spectra of the NaI-001 crystal during the first week after the arrival of the crystal underground and for a week following a 64 day interval. The peak around 50-keV is due to  $^{210}\text{Pb}$  decay inside the crystal. (b) The difference between the initial and the delayed energy spectra, which shows short life-time cosmogenic activations.

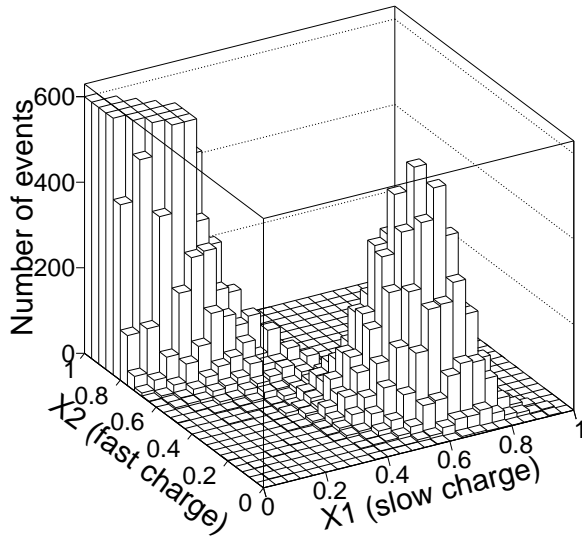
### 6.1. Accidental background from dark current

All PMTs normally have some level of dark current; this is essentially due to SPEs that are spontaneously emitted from the photocathode. In the PMTs used in these measurements, the SPE rates vary from PMT to PMT, and are typically of order  $\sim 1$  kHz. The accidental rate of two dark-current SPEs from two PMTs within 200 ns is  $\sim 0.2$  Hz. These accidental events generally have a very low charge but, because of the large variation in the charge registered for a SPE, the energy could occasionally be  $>1$  keV. Therefore, we require at least

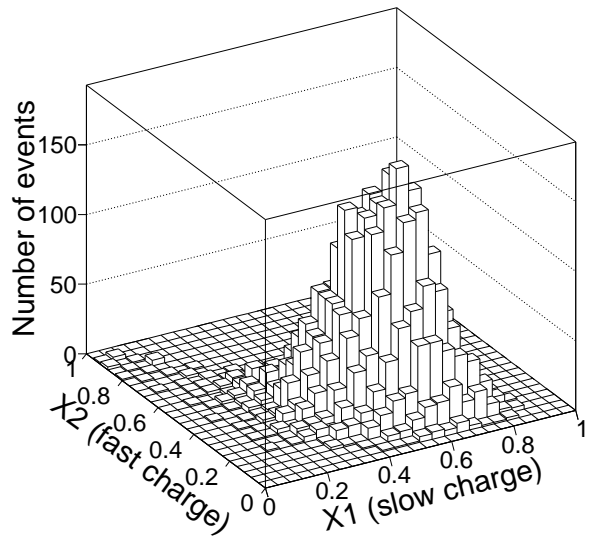
two PEs in both PMTs to reject events from dark-current-induced accidentals.

### 6.2. DAMA cut

The DAMA group reported a signal selection criteria for efficiently removing the PMT noise events from their NaI(Tl) detectors that exploits the fact that noise pulses are generally fast. The DAMA requirement places restrictions on the ratio of “fast” charge (0–50 ns), X1, and “slow” charge (100–600 ns), X2 [32, 34]. We examined the DAMA parameters for our NaI(Tl) crystals. Figure 12 shows



(a) Background data



(b)  $^{55}\text{Fe}$  calibration data

Figure 12: Two-dimensional plots of “fast” and “slow” charges for background (a) and low-energy x-ray source calibration (b) data. PMT noise events have larger “fast” charges and signal events have larger “slow” charges.

a two-dimensional  $X_2$  *versus*  $X_1$  scatter-plot for events in the 2–4 keV energy range both for background data (a) and for data taken with an  $^{55}\text{Fe}$  source (b). The figure shows that our discrimination between noise and signal is very efficient, similar to the DAMA results [34]. A rejection rate of the 2–4 keV WIMP search data is approximately 84%, however approximately 86% of the  $\sim 3$  keV  $^{40}\text{K}$  coincidence events is remained.

### 6.3. Asymmetry cut

Although a large fraction of PMT noise events below 5 keV are removed by the DAMA requirement, we find that some PMT noiselike events remain. We, therefore, developed further requirements to remove these events. We define the asymmetry between the two PMT signals as

$$\text{asymmetry} \equiv \frac{Q_1 - Q_2}{Q_1 + Q_2}, \quad (3)$$

where  $Q_1$  and  $Q_2$  are the charges measured by the two PMTs. This asymmetry allows us to locate where the event occurred inside the crystal. A similar study of asymmetry cuts with NaI crystals was reported previously [37].

To characterize PMT noiselike events, we used multiple hit events in which two or more detector

modules satisfy the trigger condition. Figure 13 shows a two-dimensional asymmetry *versus* energy scatter plot for single-hit (a) and multiple-hit (b) events. These data are obtained from the NaI-001 crystal coupled with R12669 PMTs. In the data shown in these figures, the DAMA requirement has already been applied. The multiple-hit events have  $|\text{asymmetry}| < 0.6$ , while many single-hit events with energy below 3 keV have asymmetries that are even larger than those for real events that occur near the edge of the crystal. This suggests that these events are caused by visible light produced near one of the PMTs. In contrast, the NaI-002 detector with the R11065 metal PMTs do not show many events with such large asymmetries. Events with  $|\text{asymmetry}| > 0.6$  are rejected.

### 6.4. Cluster charge cut

We found a peculiar class of low energy events in the single hit sample that are made up of SPE clusters that are spread nearly uniformly over a few hundred nanosecond interval. These are evident in the scatter-plot of the total energy *versus* the average charge of the energy clusters (total charge/number of clusters) shown in Fig. 14, where the black dot entries are for single-hit events and the red circles are for multiple-hit events. These

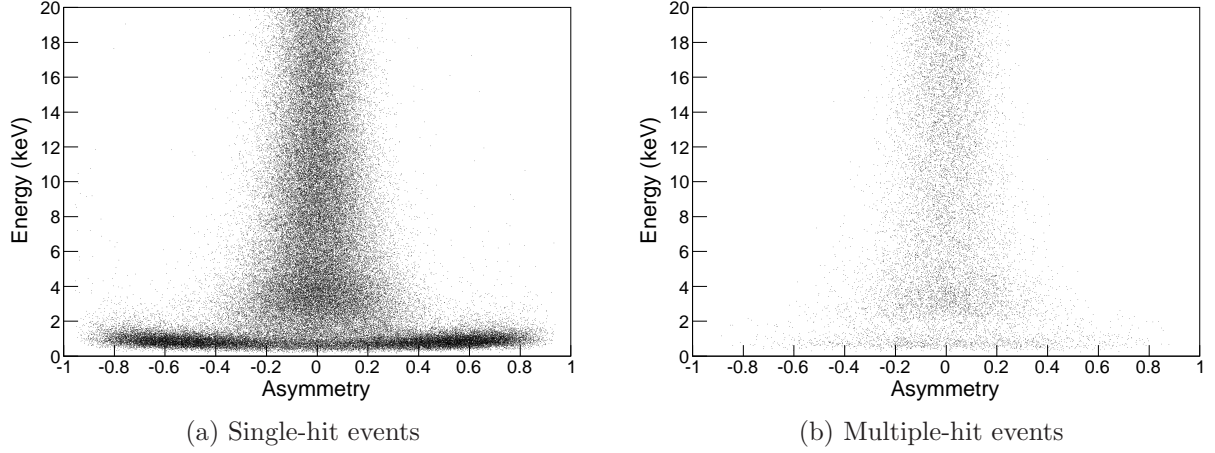


Figure 13: Asymmetry *versus* energy plots of the NaI-001 coupled with an R12669 PMT for single-hit events (a) and multiple-hit events (b). Many single-hit events with energy below 3 keV have large asymmetries that are attributed to PMT noise.

data were obtained with the NaI-001 crystal coupled to the glass R12669 PMTs, and the DAMA and asymmetry selection requirements were applied. A distinct cluster of low energy signals with an average cluster charge consistent with that for a SPE shows up for single-hit events. While the source of these events is still not understood, since they do not show up in multiple hit events, they are considered likely to be induced by PMT-noise. Although this phenomenon requires additional study, for now we veto events that lie to the left of the solid curve shown in the figure.

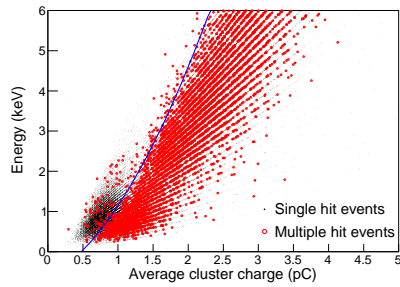


Figure 14: Energy versus the average charge of clusters for single-hit events (dots) and multiple-hit events (open circles). There are additional noise events for the single-hit events in lower cluster charge regions. The solid line shows the cut condition to remove such noise events.

## 7. Background model

Figure 15 shows the background levels of the two crystals coupled to R12669 PMTs after the application of all of the event selection criteria discussed before. NaI-002 has a much lower background level than that of NaI-001, because of its lower cosmogenic activation as a result of its surface delivery and its lower  $^{210}\text{Pb}$  contamination. Its background level at 6 keV is  $\sim 3$  counts/kg/keV/day. The figure also shows that the new PMTs with higher quantum efficiency may enable us to lower the energy threshold to near 1 keV if we have an additional understanding of the PMT noise below 2 keV.

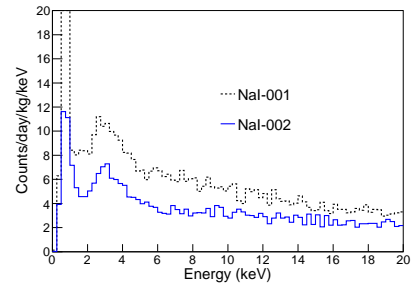


Figure 15: Background levels in the two crystals after the application of the PMT noise rejection requirements. Here we show data obtained with the R12669 glass PMTs.



### 7.1. Background simulations

We simulated the background spectra with Geant4-based detector simulations of  $^{210}\text{Pb}$ ,  $^{238}\text{U}$ ,  $^{232}\text{Th}$ , and  $^{40}\text{K}$  with contamination levels set at the measured values for each crystal. Figure 16 shows the data and the simulated spectra for the two crystals. For the current NaI(Tl) crystals, the significant remaining backgrounds are from  $^{210}\text{Pb}$ ,  $^{40}\text{K}$ , and PMT noise. The U, Th, and Ra internal contamination levels in the crystal produce backgrounds at low energies that are already sufficiently small: *i.e.*  $<0.1$  counts/keV/kg/day. The measured background levels of NaI crystals for energies below 10 keV is higher than that of the internal background simulation by  $\sim 2$  counts/keV/kg/day. This difference is attributed to  $\gamma$ -rays from sources that are exterior to the crystal, *i.e.*, the PMTs, the surrounding CsI crystals, and the materials of the surrounding shield. In addition to these constant backgrounds, there are also  $^{125}\text{I}$  and  $^{125}\text{Te}$  cosmogenic backgrounds that are continuously decreasing as a function of time. Further simulations will clarify and quantify the contributions from each external source as well as the contributions from cosmogenic activations to the total background level.

## 8. Perspectives

The DAMA experiment has been consistently showing a significant annual modulation with two different experimental arrangements that has persisted over the past 15 years. To check these results, it is necessary to use the same target material and preferable to have a lower threshold and reduced background levels. Achieving a software energy threshold of 1 keV seems feasible because of the high crystal light output and the high quantum efficiency of the new PMTs. Background levels can be significantly improved from the current measured background level of  $\sim 3$  counts/keV/kg/day (at 6 keV) by growing the crystals from purer NaI powder and in a Rn-free environment. Because the main internal backgrounds are due to  $^{210}\text{Pb}$  and  $^{40}\text{K}$ , we are attempting to reduce these contaminations below the background level of 0.2 counts/keV/kg/day for each source, and the prospects of starting with purer powder from Sigma Aldrich<sup>4</sup> are promising.

---

<sup>4</sup><http://www.sigmaaldrich.com>

In addition to the internal backgrounds, the external backgrounds need to be controlled well below 0.5 counts/keV/kg/day. Low-background, metal-housed PMTs with lower radioactivity specifications are commercially available and it is possible to use high efficiency SBA photocathodes with these tubes. We are working closely with the Hamamatsu Company to develop a PMT that is better suited for a low-background NaI(Tl) crystal detector module.

Further, we expect a significant reduction in the internal or external backgrounds by the immersion of the NaI(Tl) crystal array inside a liquid scintillator box that provides an active veto capability. A naive simulation shows that  $\sim 70\%$  of the PMT-initiated backgrounds below 10 keV can be vetoed. A performance test with a single NaI crystal is in progress.

## 9. Conclusion

We tested the performance of two large NaI(Tl) crystals as part of a program to develop ultra-low-background NaI crystals for WIMP searches. We developed selection requirements that are effective for reducing PMT-noise induced background signals. Based on this effort, we achieved a background level of  $\sim 3$  counts/keV/kg/day at 6 keV and a  $<2$  keV energy threshold. A number of efforts are being pursued that are aimed at further reduction of these backgrounds. The successful development of ultra-low-background and low-energy-threshold NaI crystals with much reduced PMT background will guarantee a definitive and unambiguous test of the DAMA experiment's annual modulation signal.

## Acknowledgments

We thank the Korea Hydro and Nuclear Power (KHNP) company for providing the underground laboratory space at Yangyang. This research was funded by Grant No. IBS-R016-D1 and was supported by the Basic Science Research Program through the National Research Foundation of Korea (NRF) funded by the Ministry of Education (NRF-2011-35B-C00007).

## References

- [1] E. Komatsu *et al.* (WMAP Collaboration), *Astrophys. J. Suppl.* 192 (2011) 18.
- [2] P. A. R. Ade *et al.* (Planck Collaboration), *arXiv:1303.5076*.

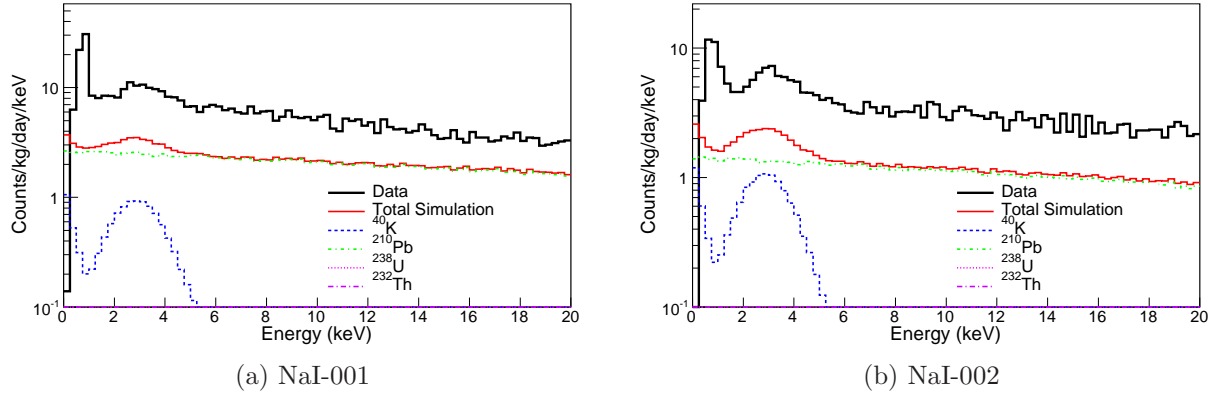


Figure 16: The measured background levels in the NaI crystals compared with simulations of backgrounds from internal contamination in the crystals.

- [3] B. W. Lee and S. Weinberg, Phys. Rev. Lett. 39 (1977) 165.
- [4] G. Jungman, A. Kamionkowski, and K. Griest, Phys. Rep. 267 (1996) 195.
- [5] R. Gaitskell, Annu. Rev. Nucl. Part. Sci. 54 (2004) 315.
- [6] L. Baudis, Phys. Dark Univ. 1 (2012) 94.
- [7] R. Bernabei *et al.* (DAMA Collaboration), Eur. Phys. J. C 56 (2008) 333.
- [8] R. Bernabei *et al.* (DAMA Collaboration), Eur. Phys. J. C 67 (2010) 39.
- [9] R. Bernabei *et al.* (DAMA Collaboration), Eur. Phys. J. C 73 (2013) 2648.
- [10] C. E. Aalseth *et al.* (CoGeNT Collaboration), Phys. Rev. Lett. 107 (2011) 141301.
- [11] C. E. Aalseth *et al.* (CoGeNT Collaboration), Phys. Rev. D 88 (2013) 012002.
- [12] C. E. Aalseth *et al.* (CoGeNT Collaboration), arXiv:1401.3295.
- [13] G. Angloher *et al.* (CRESST Collaboration), Eur. Phys. J. C 72 (2012) 1971.
- [14] R. Agnese *et al.* (CDMS Collaboration), Phys. Rev. Lett. 111 (2013) 251301.
- [15] Q. Yue *et al.* (CDEX Collaboration), arXiv:1404.4946.
- [16] G.K. Giovanetti *et al.*, arXiv:1407.2238.
- [17] G. Angloher *et al.* (CRESST Collaboration), arXiv:1407.3146.
- [18] E. Aprile *et al.* (XENON100 Collaboration), Phys. Rev. Lett. 109 (2012) 181301.
- [19] R. Agnese *et al.* (SuperCDMS Collaboration), Phys. Rev. Lett. 112 (2014) 041302.
- [20] D. S. Akerib *et al.* (LUX Collaboration), Phys. Rev. Lett. 112 (2014) 091303.
- [21] G. Plante *et al.*, Phys. Rev. C 84 (2011) 045805.
- [22] D. Barker and D. M. Mei, Astropart. Phys. 38 (2012) 1.
- [23] Y. Y. Mao, L. E. Strigari, and R. H. Wechsler, Phys. Rev. D 89 (2014) 063513.
- [24] J. Amare *et al.*, Nucl. Instrum. Methods Phys. Res., Sect. A 742 (2014) 187.
- [25] J. Amare *et al.*, arXiv:1404.3564.
- [26] J. Cherwinka *et al.* (DM-Ice Collaboration), arXiv:1401.4804.
- [27] Y. D. Kim *et al.*, J. Korean. Phys. Soc. 40 (2002) 520; Y. D. Kim *et al.*, Nucl. Instrum. Methods Phys. Res., Sect. A 552 (2005) 456.
- [28] T. Y. Kim *et al.*, Nucl. Instrum. Methods Phys. Res., Sect. A 500 (2003) 337; H. S. Lee *et al.*, Nucl. Instrum. Methods Phys. Res., Sect. A 571 (2007) 644.
- [29] H. S. Lee *et al.*, (KIMS Collaboration), Phys. Rev. Lett. 99 (2007) 091301.
- [30] S. C. Kim *et al.*, (KIMS Collaboration), Phys. Rev. Lett. 108 (2012) 181301.
- [31] J. J. Zhu *et al.*, High Energ. Phys. Nucl. 29 (2005) 8.
- [32] R. Bernabei *et al.*, JINST 7 (2012) P03009.
- [33] H. S. Lee *et al.* (KIMS Collaboration), Phys. Lett. B 633 (2006) 201.
- [34] R. Bernabei *et al.*, Nucl. Instrum. Methods Phys. Res., Sect. A, 592 (2008) 297.
- [35] S. Agostinelli *et al.*, Nucl. Instrum. Methods Phys. Res., Sect. A 506 (2003) 250; J. Allison *et al.*, IEEE Tran. Nucl. Sci. 53 (2006) 270.
- [36] C. Cuesta *et al.*, arXiv:1403.3580.
- [37] M. Robinson *et al.*, Nucl. Instrum. Methods Phys. Res., Sect. A, 545 (2005) 225.